2000 days), with planet occurrence varying as $df \propto M^{-0.31 \pm 0.2} P^{0.26 \pm 0.1}$ d$\log M$ d$\log P$. Although the details of planet formation probably differ for gas-giant and terrestrial planets, we can speculate that if the trend of increasing planet occurrence with longer orbital period holds down to an Earth mass, then $\eta_{\mathrm{Earth}} = 23\%$ is an underestimate for orbits near 1 AU. For orbits beyond the ice line (~2.5 AU), gravitational microlensing searches find three times as many Neptunes as Jupiters (*28*), suggesting that planet occurrence also increases with decreasing planet mass in this domain.

The distribution of planets in the mass/orbital-period plane (Fig. 1) reveals important clues about planet formation and migration. Planets with $M \sin i = 10$ to 100 M_{Earth} and $P < 20$ days are almost entirely absent. There is also an overdensity of planets starting at $P < 10$ days and $M \sin i = 4$ to 10 M_{Earth} and extending to higher masses and longer periods. These patterns suggest different formation and migration mechanisms for close-in low-mass planets as compared to massive gas-giant planets.

Population synthesis models of planet formation predict an increase in planet occurrence with decreasing planet mass (*2*, *29*). However, the bulk of their predicted low-mass planets reside near the ice line, well outside of the $P < 50$ days domains analyzed here. In fact, these models predict a "planet desert" precisely in the domain of mass and period where we detect an overdensity of planets. The desert emerges naturally in the simulations (*3*, *4*) from fast migration and accelerating planet growth. Most planets are born near or beyond the ice line, and those that grow to a critical mass of several Earth masses either rapidly spiral inward to the host star or undergo runaway gas accretion and become massive gas giants. Our measurements show that population synthesis models of planet formation are currently inadequate to explain the distribution of low-mass planets.

The Kepler mission (*30*) is currently surveying 156,000 faint stars for transiting planets as small as Earth. Our power-law model predicts that Kepler will detect a bounty of close-in small planets: an occurrence rate of 22% for $P < 50$ days and $M \sin i = 1$ to 8 M_{Earth}, corresponding to 1 to 2 Earth radii, assuming terrestrial, Earth-like density (5.5 kg m^{-3}). When the mission is complete, we estimate (see SOM) that Kepler will have detected the transits of 120 to 260 of these plausibly terrestrial worlds orbiting the ~10^4 G and K dwarfs brighter than 13th magnitude (*31*, *32*).

References and Notes

1. S. Ida, D. N. C. Lin, *Astrophys. J.* **604**, 388 (2004).
2. S. Ida, D. N. C. Lin, *Astrophys. J.* **626**, 1045 (2005).
3. S. Ida, D. N. C. Lin, *Astrophys. J.* **685**, 584 (2008).
4. C. Mordasini, Y. Alibert, W. Benz, *Astron. Astrophys.* **501**, 1139 (2009).
5. A. W. Howard *et al.*, *Astrophys. J.* **696**, 75 (2009).
6. S. S. Vogt *et al.*, *Proc. SPIE Instrum. Astron. VIII* **2198**, 362 (1994).
7. A. W. Howard *et al.*, *Astrophys. J.*, available at http://arxiv.org/abs/1003.3444 (2010).
8. J. A. Johnson *et al.*, *Proc. Astron. Soc. Pacific* **122**, 149 (2010).
9. R. P. Butler *et al.*, *Astrophys. J.* **646**, 505 (2006).
10. D. A. Fischer, G. W. Marcy, R. P. Butler, G. Laughlin, S. S. Vogt, *Astrophys. J.* **564**, 1028 (2002).
11. M. Mayor, D. Queloz, *Nature* **378**, 355 (1995).
12. D. A. Fischer *et al.*, *Astrophys. J.* **675**, 790 (2008).
13. S. S. Vogt *et al.*, *Astrophys. J.* **708**, 1366 (2010).
14. G. W. Marcy, R. P. Butler, *Astrophys. J.* **464**, L147 (1996).
15. E. J. Rivera *et al.*, *Astrophys. J.* **708**, 1492 (2010).
16. R. A. Wittenmyer, M. Endl, W. D. Cochran, H. F. Levison, G. W. Henry, *Astrophys. J. Suppl. Ser.* **182**, 97 (2009).
17. C. Lovis *et al.*, *Nature* **441**, 305 (2006).
18. D. Fischer *et al.*, *Astrophys. J.* **703**, 1545 (2009).
19. C. Mordasini *et al.*, *Astron. Astrophys.*, available at http://arxiv.org/abs/1010.0856.
20. J. T. Wright *et al.*, *Astrophys. J.* **683**, L63 (2008).
21. J. T. Wright *et al.*, *Astrophys. J.* **693**, 1084 (2009).
22. S. S. Vogt *et al.*, *Astrophys. J.* **632**, 638 (2005).
23. G. Marcy *et al.*, *Prog. Theor. Phys.* **158** (suppl.), 24 (2005).
24. S. J. O'Toole *et al.*, *Astrophys. J.* **701**, 1732 (2009).
25. M. Mayor *et al.*, *Astron. Astrophys.* **493**, 639 (2009).
26. M. Mayor, 2010, KITP Conference: Exoplanets Rising: Astronomy and Planetary Science at the Crossroads, an online presentation at the Kavli Institute for Theoretical Physics, Santa Barbara, CA, 29 March 2010, www.portaltotheuniverse.org/podcasts/eps/view/53704/.
27. A. Cumming *et al.*, *Proceedings of the Astronomical Society of the Pacific* **120**, 531 (2008).
28. T. Sumi *et al.*, *Astrophys. J.* **710**, 1641 (2010).
29. C. Mordasini, Y. Alibert, W. Benz, D. Naef, *Astron. Astrophys.* **501**, 1161 (2009).
30. W. J. Borucki *et al.*, *Science* **327**, 977 (2010).
31. N. M. Batalha *et al.*, *Astrophys. J.* **713**, L109 (2010).
32. W. J. Borucki *et al.*, *Astrophys. J.*, available at http://arxiv.org/abs/1006.2799 (2010).

33. This work was based on observations at the W. M. Keck Observatory granted by NASA and the University of California (UC). We thank the many observers who contributed to the measurements reported here and acknowledge the efforts and dedication of the Keck Observatory staff, especially S. Dahm, H. Tran, and G. Hill for support of HIRES and G. Wirth for support of remote observing. We acknowledge R. P. Butler and S. Vogt for many years of contributing to the data presented here. A.H. acknowledges support from a Townes Postdoctoral Fellowship at the UC Berkeley Space Sciences Laboratory. G.M. acknowledges NASA grant NNX06AH52G. Finally, we extend special thanks to those of Hawai'ian ancestry on whose sacred mountain of Mauna Kea we are privileged to be guests.

Supporting Online Material

www.sciencemag.org/cgi/content/full/330/6004/653/DC1
Materials and Methods
Figs. S1 to S7
Tables S1 to S3
References

8 July 2010; accepted 27 September 2010
10.1126/science.1194854

Transferable GaN Layers Grown on ZnO-Coated Graphene Layers for Optoelectronic Devices

Kunook Chung,[1] Chul-Ho Lee,[1,2] Gyu-Chul Yi[1]*

We fabricated transferable gallium nitride (GaN) thin films and light-emitting diodes (LEDs) using graphene-layered sheets. Heteroepitaxial nitride thin films were grown on graphene layers by using high-density, vertically aligned zinc oxide nanowalls as an intermediate layer. The nitride thin films on graphene layers show excellent optical characteristics at room temperature, such as stimulated emission. As one of the examples for device applications, LEDs that emit strong electroluminescence emission under room illumination were fabricated. Furthermore, the layered structure of a graphene substrate made it possible to easily transfer GaN thin films and GaN-based LEDs onto foreign substrates such as glass, metal, or plastic.

Inorganic compound semiconductors such as gallium arsenide (GaAs) and gallium nitride (GaN) provide many advantages over organic materials for optoelectronic device applications, including high carrier mobility and radiative recombination rates, as well as long-term stability and reliability (*1*, *2*). However, problems associated with high-quality inorganic film growth on large or flexible substrates represent one of the major obstacles to the use of inorganic semiconductors in foldable-display and solar-cell applications. Previous techniques such as epitaxial growth and lift-off circumvent this problem by separation of the thin film from the growth substrates (*3*–*6*), but difficulty in separating the film from a single-crystal substrate limits their use. Meanwhile, the layered structure of graphene sheets, which consist of weakly bonded layers of hexagonally arranged carbon atoms held together by strong covalent bonds, makes it easy to transfer the film to foreign substrates. Here, we describe the methods to grow a high-quality, epitaxial GaN layer and fabricate $In_xGa_{1-x}N$/GaN multi-quantum-well (MQW)–structure light-emitting diodes (LEDs) on graphene layers. Furthermore, the LEDs were transferred onto foreign substrates, such as metal, glass, and plastic, and exhibited strong light emission even under room illumination.

[1]National Creative Research Initiative Center for Semiconductor Nanorods and Department of Physics and Astronomy, Seoul National University, Seoul 151-747, South Korea. [2]Department of Materials Science and Engineering, Pohang University of Science and Technology, Pohang, Gyeongbuk 790-784, South Korea.

*To whom correspondence should be addressed. E-mail: gcyi@snu.ac.kr

Because of the excellent optical and electrical characteristics of nitride semiconductors, full-color-spectrum nitride LEDs with high efficiency and reliability and long-term stability are now commercially available (*7*). Nevertheless, problems of limited substrate size, high cost, high-resistance ohmic contacts, and poor heat dissipation remain, primarily because of the requirement of a sapphire substrate for nitride film growth. Additionally, for large-area or flexible-device applications, the device must be fabricated on glass, plastic, or metal substrates. However, high-quality, epitaxial nitride films can be grown only on a lattice-matched single-crystal substrate at a high growth temperature, above 1000°C (*1*); glass and plastic substrates have no tolerance for such high temperatures and, as amorphous materials, cannot be used for epitaxial growth of a crystalline film (*8*). For this reason, previous techniques—most notably epitaxial growth and lift-off—have separated thin films from their growth substrates to make flip-chip devices on metal substrates (*3*–*6*). However, difficulties in separating the films from a single-crystal substrate arising from strong bonding between GaN and sapphire and their high mechanical and chemical stability have limited the use of such techniques. This difficulty can be resolved readily by using substrates composed of graphene layers because the graphene-layer structure makes it possible to transfer the epitaxial film grown on graphene layers to substrates such as metal, glass, and plastic. As recently reported, large graphene films that exhibit high-temperature stability, optical transparency, mechanical flexibility, and electrical and thermal conductivities are now available (*9*, *10*).

The basic strategy for epitaxial growth of GaN on graphene layers is shown in Fig. 1 (*11*). A mirror-smooth, epitaxial GaN thin film could not be grown on pristine graphene layers, presumably because of the lack of chemical reactivity. Although GaN nucleation would not occur on the basal plane of pristine graphene, GaN islands can be grown readily along the naturally formed step-edges (fig. S1A). Accordingly, the first step is to create many step-edges, which can then act as nucleation sites. Oxygen-plasma treatment can make graphene rough (*12*). Meanwhile, although the oxygen-plasma treatment increased the GaN island density, GaN films were polycrystalline, and their surfaces were rough and irregular (fig. S1B), which is similar to the previous report on GaN films that were grown on graphite substrates (*8*). Even the typical use of a low-temperature GaN buffer layer did not improve the film crystallinity or morphology. Thus, we grew high-density zinc oxide (ZnO) nanowalls on oxygen-plasma–treated graphene layers: an intermediate layer for GaN growth. Figure 1, C and D, shows scanning electron microscopy (SEM) images of high-density, epitaxial ZnO nanowalls grown on plasma-treated graphene layers and a GaN thin film on the nanowalls, respectively. As previously reported (*13*), ZnO nanowalls are grown along naturally formed graphene step-edges, and accordingly, step-edges generated by oxygen-plasma lead to the formation of high-density ZnO nanowalls. Because of the same crystal structure and small lattice misfits with GaN, epitaxial GaN films grow on the nanowalls by means of lateral overgrowth. Although the lateral overgrowth depended on the nanowalls density (fig. S3), the SEM image in Fig. 1D shows the flat surface morphology. The high-density ZnO nanowalls play a critical role in the heteroepitaxial growth of GaN on graphene layers.

We obtained photoluminescence (PL) spectra (Fig. 2) of GaN thin films grown on graphene layers at room temperature using a continuous-wave helium-cadmium (He-Cd) or pulsed neodymium-doped yttrium aluminum garnet (Nd:YAG) laser as the optical excitation source. At a low excitation power of 1 W/cm^2 with a He-Cd laser, the dominant PL emission peak was at 3.40 eV, and a very weak deep-level emission was at 2.2 eV, which correspond to near-band-edge (NBE) emission associated with excitons and deep levels, respectively. This strong NBE emission with the extremely low deep-level emission indicates the high optical quality of GaN films on graphene layers. For low excitation power with the pulsed Nd:YAG laser [below a threshold value (I_{th}) of 0.6 MW/cm^2], the broad NBE emission peak was still observed at 3.40 eV, which is quite similar to that measured by using a He-Cd laser, although a shoulder was also seen at 3.34 eV. The integrated intensity increased linearly with the pumping power, indicating that the observed peak originated from the spontaneous emission. However, for excitation power above I_{th}, a very sharp and strong PL emission at 3.29 eV predominated that evolved from the low-energy shoulder of the spontaneous emission. Furthermore, the integrated PL intensity increased superlinearly with the pumping power, providing evidence of the stimulated emission. The threshold pumping power of 0.6 MW/cm^2, estimated from the inset in Fig. 2, is similar to the previously reported values of 0.56 to 0.70 MW/cm^2 for GaN thin films on sapphire, silicon (Si), and silicon carbide (SiC) substrates (*14*–*16*).

The heteroepitaxial growth of a high-quality thin film on graphene layers provides a hybrid heterostructure of a three-dimensional bulk single-crystal and a two-dimensional molecular material. When we use graphene layers as a substrate for the heteroepitaxial growth, a potential major advantage is that lattice mismatch may not be considered seriously because the graphene layers have weak bonding to each other. As determined with x-ray diffractometry and transmission elec-

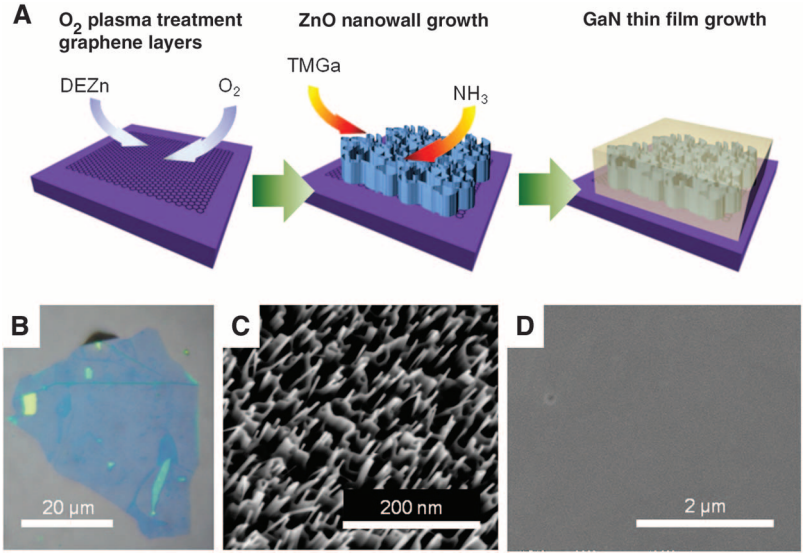

Fig. 1. (**A**) Schematic illustrations of fabrication processes for epitaxial GaN thin films. (**B**) Optical microscopic image of oxygen-plasma–treated graphene layers. (**C** and **D**) SEM images of (C) ZnO nanowalls grown on plasma-treated graphene layers and (D) GaN thin film grown on ZnO nanowalls on plasma-treated graphene layers.

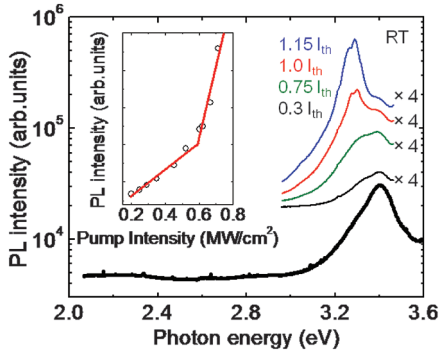

Fig. 2. Room-temperature PL spectra of GaN thin films grown on graphene layers. The thick black line and thin color lines represent the PL spectrum measured by using a continuous-wave He-Cd laser and the power-dependent PL spectra by using a pulsed Nd:YAG laser, respectively. (**Inset**) The integrated emission intensity as a function of the optical excitation.

tron microscopy, GaN films grown on graphene layers are of high crystallinity (figs. S4 and S5). The layered graphene substrates also allow transfer of the thin films onto foreign substrates and for the graphene layers to serve as electrode materials.

Schematic diagrams of the fabrication of GaN thin-film LEDs on graphene layers and their transfer onto foreign substrates are shown in Fig. 3A. To fabricate LED structures, a 2-μm-thick layer of Si-doped *n*-GaN, three-period $In_xGa_{1-x}N$/GaN MQWs, and a 350-nm-thick layer of Mg-doped *p*-GaN were deposited on the flat GaN film grown on graphene layers. For the electroluminescent (EL) devices, the metallic graphene layers underneath *n*-GaN and nickel/gold (Ni/Au) bilayers deposited on the top surface of *p*-GaN were used as *n*- and *p*-type contacts, respectively. After fabricating the devices, thin-film LEDs on the graphene layers were removed mechanically from the original substrate and transferred onto foreign substrates of metal, glass, and plastic.

All transferred devices emitted very strong blue light emissions that could be seen with unaided eyes under normal room illumination. As shown in the optical microscopy image in Fig. 3B, the light emission was fairly uniform over the area of 300 μm by 300 μm, presumably because of uniform current spreading and injection through the metallic bottom electrode—composed of graphene layers—used in this device geometry. Each substrate in Fig. 3B has benefits for LED applications. Metal substrates provide good thermal and electrical conductivity for high-power LEDs, whereas a glass or plastic substrate may allow inorganic LEDs to be fabricated as large-area, full-color LED displays in flexible or stretchable forms. Furthermore, GaN-based epitaxial films on graphene layers may readily be used as functional components of photovoltaic devices.

The EL characteristics of the LED transferred onto plastic were investigated further by measuring power-dependent EL spectra and optical images of emissions at room temperature. The EL spectra and corresponding EL images of the LED at various applied current levels are shown in Fig. 4A. The LED light emission images and the EL spectra show an increase of emission intensity with the applied current levels of 5.1, 6.4, and 8.1 mA. We also observed that the dominant peak shifted from 2.71 to 2.75 eV as the applied current level increased from 1.7 to 8.1 mA. This blue shift can be explained in terms of both a band-filling effect of the localized energy states and a screening effect by the internal polarization electric field typically observed in LEDs with GaN/$In_{1-x}Ga_xN$ MQW structures grown on a polar surface of GaN(0001) (*17*).

In addition to the EL characteristics, the electrical characteristics of the transferable LEDs were investigated by measuring their current-voltage (*I-V*) characteristic curves. The *I-V* characteristic curve of the transferred LED onto plastic in Fig. 4B shows a good rectifying behavior with a turn-on voltage of 4.5 V and a leakage current of 1×10^{-5} A at –4 V, which is similar to those of the as-fabricated LED. However, compared with conventional GaN thin-film LEDs prepared on sapphire substrates the turn-on voltage was slightly higher because of energy barriers at the junctions between the three-material system of graphene, ZnO, and GaN.

Epitaxial nitride thin films grown on graphene layers exhibit both the optical characteristics of the compound semiconductor and the electrical and mechanical characteristics of the graphene layers. The transfer of the materials and devices fabricated on graphene onto foreign substrates should provide advantages in integration and design of electronics and optoelectronic devices.

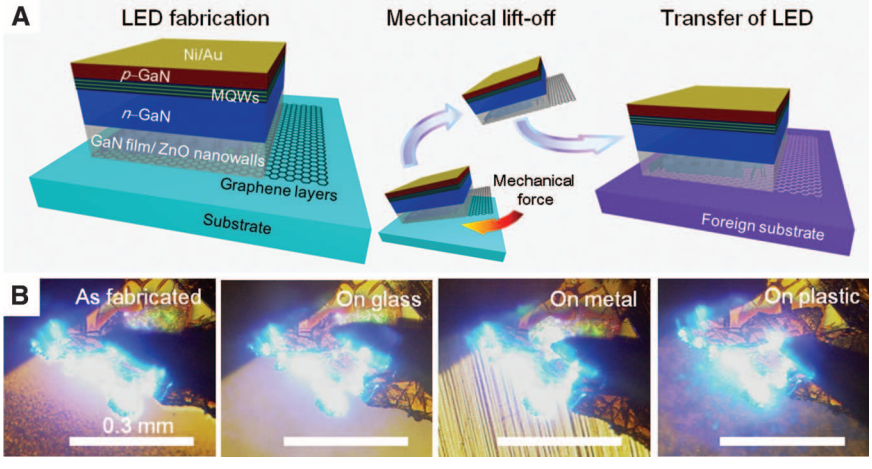

Fig. 3. (**A**) Schematic illustration of the fabrication and transfer processes for thin-film LEDs grown on graphene-layer substrates. (**B**) Optical images of light emissions from the as-fabricated LED on the original substrate and transferred LEDs on the foreign metal, glass, and plastic substrates.

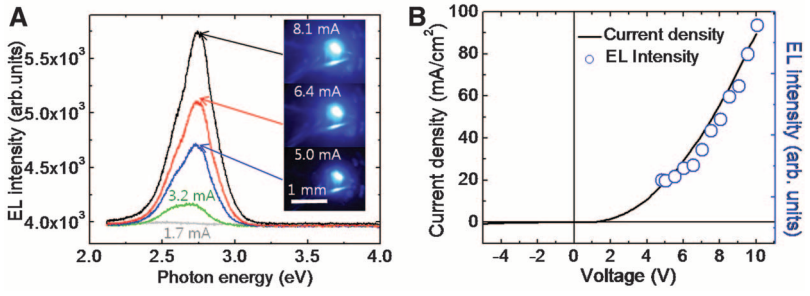

Fig. 4. (**A**) Room-temperature EL spectra of the LED transferred onto a plastic substrate. Optical microscopy images show the light emission at different applied current levels of 1.7 to 8.0 mA. (**B**) Current density and integrated EL intensity as a function of the applied bias voltage of a representative LED on a plastic substrate. The solid line and open circles correspond to the current density and integrated EL intensity, respectively.

References and Notes

1. S. Nakamura, T. Mukai, M. Senoh, *Appl. Phys. Lett.* **64**, 1687 (1994).
2. F. A. Ponce, D. P. Bour, *Nature* **386**, 351 (1997).
3. W. S. Wong, T. Sands, N. W. Cheung, *Appl. Phys. Lett.* **72**, 599 (1998).
4. W. S. Wong *et al.*, *Appl. Phys. Lett.* **75**, 1360 (1999).
5. A. David *et al.*, *Appl. Phys. Lett.* **88**, 133514 (2006).
6. H. K. Cho *et al.*, *IEEE Photon. Technol. Lett.* **20**, 2096 (2008).
7. S. Nakamura, S. Pearton, G. Fasol, *The Blue Laser Diode: The Complete Story* (Springer-Verlag, New York, ed. 2, 2000).
8. D. P. Bour *et al.*, *Appl. Phys. Lett.* **76**, 2182 (2000).
9. K. S. Kim *et al.*, *Nature* **457**, 706 (2009).
10. X. Li *et al.*, *Science* **324**, 1312 (2009).
11. Materials and methods are available as supporting material on *Science* Online.
12. X. Lu, H. Huang, N. Nemchuk, R. S. Ruoff, *Appl. Phys. Lett.* **75**, 193 (1999).
13. Y.-J. Kim, J. H. Lee, G.-C. Yi, *Appl. Phys. Lett.* **95**, 213101 (2009).
14. M. A. Khan, D. T. Olson, J. M. Van Hove, J. N. Kuznia, *Appl. Phys. Lett.* **58**, 1515 (1991).
15. S. Bidnyk *et al.*, *J. Appl. Phys.* **85**, 1792 (1999).
16. G. P. Yablonskii *et al.*, *Phys. Status Solidi A Appl. Mat.* **192**, 54 (2002).
17. E. Kuokstis *et al.*, *Appl. Phys. Lett.* **80**, 977 (2002).

18. This work was financially supported by the National Creative Research Initiative Project (grant R16-2004-004-01001-0) of the Korea Science and Engineering Foundations (KOSEF). G.-C.Y. planned the project; K.C. designed and progressed the experiments; C.-H.L. provided technical support for LED device fabrication and characterization; G.-C.Y. advised on the project; and all authors analyzed the data, interpreted the results, and wrote the manuscript. The authors declare that they have no competing financial interests.

Supporting Online Material

www.sciencemag.org/cgi/content/full/330/6004/655/DC1
Materials and Methods
Figs. S1 to S6
References

21 July 2010; accepted 27 September 2010
10.1126/science.1195403